W. -T. Hsu, J. R. Clark, and C. T. -C. Nguyen, "*Q*-optimized lateral free-free beam micromechanical resonators," *Digest of Technical Papers*, the 11th Int. Conf. on Solid-State Sensors & Actuators (Transducers'01), Munich, Germany, June 10-14, 2001, pp. 1110-1113.

Q-Optimized Lateral Free-Free Beam Micromechanical Resonators

Wan-Thai Hsu, John R. Clark, and Clark T.-C. Nguyen
Center for Wireless Integrated Microsystems
Department of Electrical Engineering and Computer Science
University of Michigan, Ann Arbor, MI 48109-2122, U.S.A.

ABSTRACT

Laterally vibrating free-free beam micromechanical resonators have been demonstrated that utilize second-mode flexural supports and optimal dc-bias application to suppress anchor dissipation and thereby attain *Q*'s greater than 10,000 at 10.47 MHz, while eliminating some of the key deficiencies associated with previous vertical-mode resonators. In addition to demonstrating lateral FF-beams, this work utilizes these resonators to quantify the degree to which the use of energy isolating supports actually influences the *Q* of this device.

Keywords: resonator, high-*Q*, lateral, oscillator

I. INTRODUCTION

Recent demonstrations of vibrating micromechanical ("μmechanical") resonators with frequencies up to mid-VHF and *Q*'s in excess of 3,000 [1][2] have spurred interest in the use of these devices as high-*Q* tanks for bandpass filters and low-phase noise reference oscillators in communication transceivers and instrumentation [3]. To date, the majority of capacitively-transduced μmechanical filters have utilized vertical-mode resonators and couplers [4], mainly due to technology considerations. Specifically, the sub-μm electrode-to-resonator gaps needed to attain sufficiently low filter impedances are most easily achieved in the vertical direction in conventional surface micromachining processes.

Unfortunately, the restriction to vertical-mode operation imposes design compromises that in some cases can limit the performance of μmechanical circuits. Among the vertical-mode deficiencies that hinder performance are: (1) topography-induced frequency uncertainty; (2) lower *Q* due to larger energy dissipation through the resonator anchors; (3) fabrication complexity issues that often constrain vertical-mode resonators to be one-port devices, effectively eliminating opportunities for balanced or differential-mode operation; and (4) geometric inflexibility imposed by vertical-mode operation. Lateral operation could alleviate all of the above, plus introduce new design possibilities, such as high frequency filter networks using *longitudinal-mode* coupling beams—a key design feature that could be instrumental in achieving future GHz μmechanical filters.

Using a recent technology that makes possible lateral sub-μm gaps without the need for aggressive lithography or etching [5], this work demonstrates a laterally vibrating free-free beam ("FF-beam") μmechanical resonator that uses second-mode flexural supports and optimal dc-bias application to suppress anchor dissipation and thereby attain *Q*'s greater than 10,000 at 10.47MHz. The design and operation of this resonator are discussed, and experimental measurements are performed to quantify the degree to which the energy isolating supports influence both the *Q* and frequency of this device.

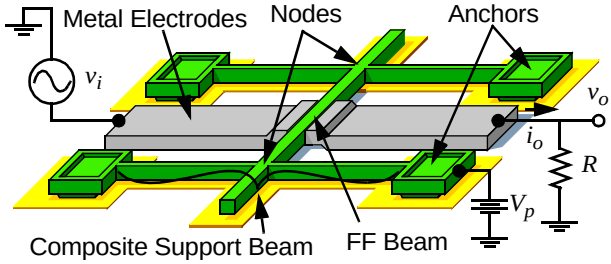

Fig. 1: Perspective-view schematic of the lateral FF-beam μmechanical resonator and test circuit.

II. DEVICE OPERATION AND DESIGN

Figure 1 presents the perspective-view schematic of the lateral FF-beam resonator in a typical measurement circuit. As shown, this resonator consists of a free-free beam suspended at its nodal locations [1] by four flexural support beams. Gold electrodes flank opposite sides of the resonator beam to allow capacitive excitation and detection of induced vibrations [4]. Although this structure looks similar to that of a previous vertical-mode counterpart [1], its design and operation is quite different. In particular, where the support beams were designed to operate in a *torsional* mode for the vertical-mode design, the support beams in Fig. 1 are designed to operate in a *lateral flexural* mode.

To suppress energy losses from the FF-beam to the support anchors, the support beams are actually designed so that the composite beams attained by combining two support beams on opposite sides of the FF-beam (from anchor-to-anchor) resonate in a second mode at the fundamental mode frequency of the FF-beam. With this design, the beam attachment locations correspond to nodal points for both the composite support beams and the FF-beam resonator, creating a high (ideally infinite) impedance location through which very little energy is transferred, hence, through which very little energy is dissipated. This allows the resonator system to attain a very high *Q*, despite the high stiffnesses of its constituent beams. Fig. 2 presents a displacement contour plot obtained via finite element simulation, showing the mode shape of the beam and supports, and verifying the lack of displacement at the nodal locations.

Free-Free Beam Design.

When the support beams are designed as described above, the expression for resonance frequency f_o of the beam in Fig. 1 takes on that for an ideal free-free beam [1]. The actual resonance frequency will actually be a

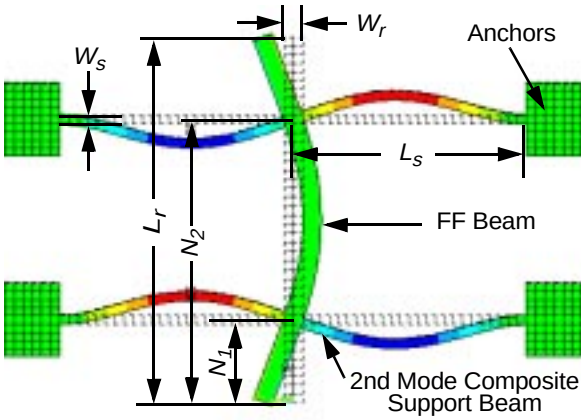

Fig. 2: Displacement contour plot of a lateral FF-beam μmechanical resonator simulated via finite-element analysis using ANSYS.

function of the electrical stiffness k_e generated through the parallel-plate capacitive transducers, and is given by

$$f_o = f_{nom}\left[1 - \langle\frac{k_{ei}}{k_m}\rangle - \langle\frac{k_{eo}}{k_m}\rangle\right]^{1/2}, \quad (1)$$

where f_{nom} is the resonance frequency (given in [1]) of an ideal FF-beam in the absence of electromechanical coupling, and $<k_{ei}/k_m>$ and $<k_{eo}/k_m>$ are mechanical-to-electrical stiffness ratios associated with the input and output electrodes, respectively, and dependent upon the values of dc-bias voltage V_P and electrode-to-resonator gap spacing d_o, as more fully detailed in [4].

Support Beam Design.

For a given FF-beam resonance frequency f_o, the composite support beams vibrate in their second modes when their lengths are chosen to satisfy

$$L_s = 1.683\left[\sqrt{\frac{E}{\rho}}\frac{W_s}{f_o}\right]^{1/2}, \quad (2)$$

where E and ρ are the Young's modulus and density, respectively, of the structural material, and W_s and L_s are indicated in Fig. 2.

III. FABRICATION

Various lateral FF-beam μmechanical resonators were designed and fabricated using a previously demonstrated technology that combines polysilicon surface micromachining, metal electroplating, and a sacrificial sidewall spacer technique to achieve μmechanical structures in a high-Q polysilicon material with low resistance (i.e., low loss) metal electrodes, and with electrode-to-resonator gaps less than 0.1μm [5]. Figure 3 presents the scanning electron micrograph (SEM) of a 10.47 MHz polysilicon lateral FF-beam resonator fabricated using this process. The inset of Fig. 3 presents a close-up SEM of the capacitive transducer, showing details of the tiny gap.

IV. EXPERIMENTAL RESULTS

Table I, along with Fig. 2, summarizes the geometric designs of 10 MHz and 20 MHz lateral FF-beam μmechanical resonators, with second-mode suspension

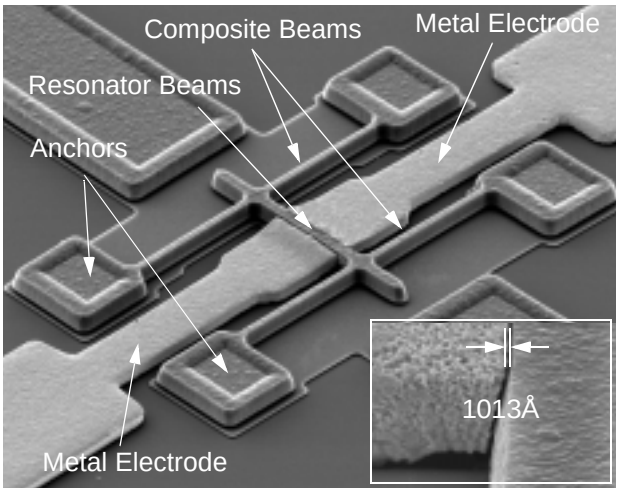

Fig. 3: SEM of a 10.47 MHz lateral FF-beam μmechanical resonator.

Table I: Lateral FF-Beam Design Summary

Design Parameters	10MHz	20MHz	unit
FF-Beam Length, L_r	39.8	28.6	μm
FF-Beam Width, W_r	2	2	μm
Support Beam Length, L_s	25.6	18.4	μm
Support Beam Width, W_s	1.2	1.2	μm
Thickness, h	2	2	μm
Electrode Width, W_e	14	9	μm
DC-bias Voltage, V_P	30	30	V
Gap Spacing, d_o	1000	1000	Å

beams designed for maximum Q, all fabricated using the lateral sub-μm process of Section III. In addition to these devices, the process run also included devices with suspension beams that deviate from optimal dimensions with the intent of exploring the impact of suspension non-idealities on performance.

A custom-built vacuum chamber with both dc and coaxial feedthroughs for connections to external instrumentation was utilized to test μmechanical devices. All devices were tested under 80μTorr vacuum provided by a turbo-molecular pump.

Lateral FF-Beam Resonator Performance.

The frequency characteristic for the 10.47 MHz resonator of Fig. 3 measured via an HP8714 Network Analyzer is shown in Fig. 4. Here, a Q of 10,741 is seen, which is significantly higher than that attainable via previous clamped-clamped beam μmechanical resonators [1]. Figure 5 presents the measured frequency characteristic for a 19.553 MHz device, again showing a very good Q of 7,306. Note that the degree of symmetry seen in both plots is much better than seen in one-port μmechanical counterparts, which suffer somewhat from the presence of a static capacitor in parallel with the resonator's *LCR* equivalent circuit. This is advantageous, since symmetry can be important in many filter and oscillator

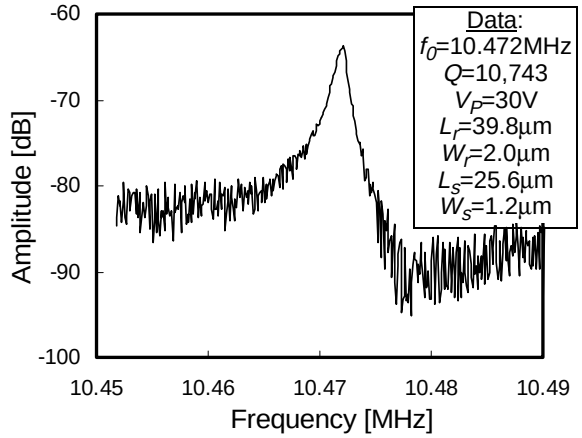

Fig. 4: Measured frequency characteristic for a 10.47 MHz lateral FF-beam µmechanical resonator

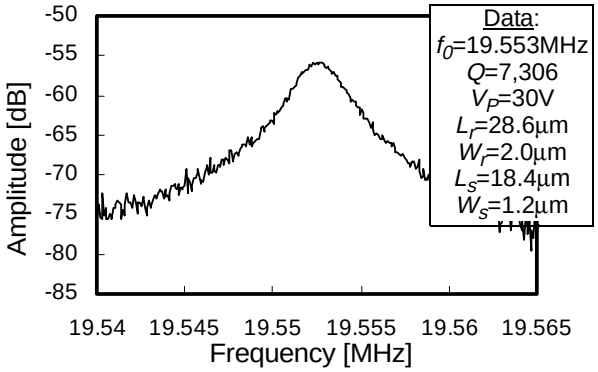

Fig. 5: Measured frequency characteristic for a 19.553 MHz lateral FF-beam µmechanical resonator

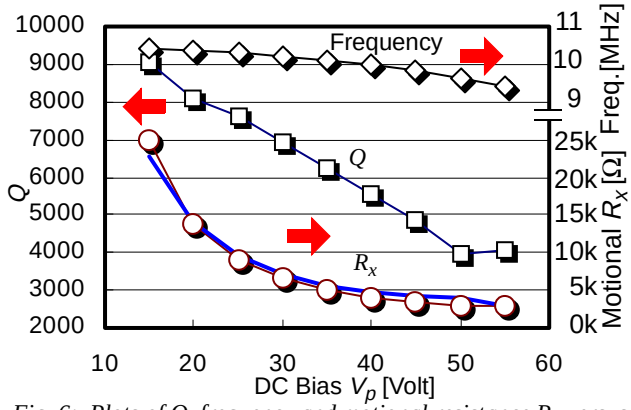

Fig. 6: Plots of Q, frequency and motional resistance R_x versus dc-bias voltage V_P for a 10 MHz lateral FF-beam µmechanical resonator.

applications, especially those requiring a balanced or differential mode of operation.

Pursuant to obtaining an accurate value for the electrode-to-resonator gap spacing d_o achieved via the lateral sub-µm gap process, Fig. 6 presents a measured plot of resonance frequency f_o versus V_P for the 10.47 MHz lateral FF-beam. By fitting these curves to (1), using the gap spacing d_o and the effective width W_{reff} of the beam as fitting parameters, the electrode-to-resonator gap spacing d_o is found to be 1050Å, which would be very

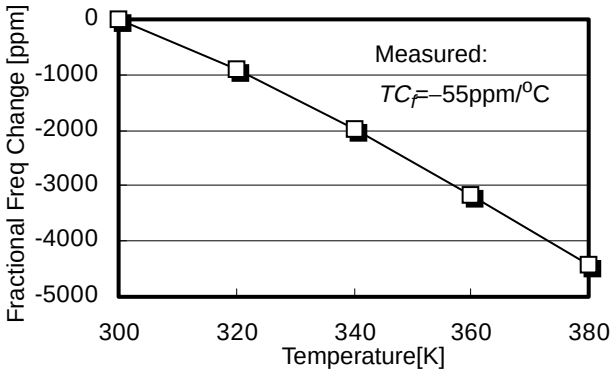

Fig. 7: Fractional frequency change versus temperature of a 10 MHz lateral FF-beam µresonator

difficult to achieve using more direct methods based on aggressive lithography (e.g., e-beam) and etching.

Using this value for d_o, the predicted curve of series motional resistance R_x [4] versus dc-bias V_P for this device is also plotted in Fig. 6, along with measured data, showing an excellent degree of matching, and attesting to the accuracy of the theory in [4]. However, the values of R_x seen in Fig. 6 are much larger than seen for previous vertical-mode µmechanical resonator devices, which can have larger electrode-to-resonator overlap areas and gaps on the order of 300Å, so routinely achieve R_x's on the order of 25Ω with similar V_P's. Given the need to match impedances to connecting blocks in communication systems, this higher value of R_x is not desirable. Fortunately, there are several immediately identifiable methods for reducing the R_x of these lateral FF-beams, some as simple as depositing more polysilicon when defining the structural material.

Temperature Dependence.

Figure 7 presents a plot of resonance frequency f_o versus temperature for the 10.47 MHz lateral FF-beam, measured by mounting the resonator die onto an MMR temperature controllable cantilever inserted into the vacuum chamber via a special port. From the slope of the curve, the temperature coefficient of the resonance frequency TC_{fo} is –55ppm/°C—more than 3 times larger than that of previous polysilicon FF-beam µmechanical resonators. The reason for such poor temperature stability stems from the use of plated-Au as the electrode material. As explained in [6], due to a combination of a tiny electrode-to-resonator gap spacing d_o and a large difference in thermal expansion coefficients between Au and the Si substrate material, the gap distance d decreases substantially from its initial value as the temperature is increased, resulting in a shift the electrical stiffness term of (1) and a consequent shift in the resonance frequency. Clearly, the use of Au electrodes in the lateral sub-µm process of [5] must be re-evaluated for applications where frequency stability is important.

Isolating Support Performance.

To quantify the degree to which the isolating supports contribute to the observed high Q, Fig. 6 also includes a

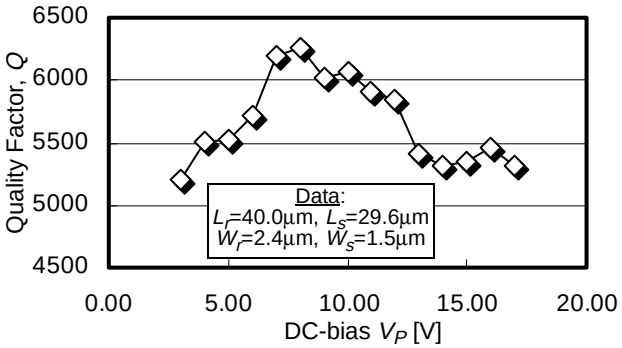

Fig. 8: Q versus dc-bias voltage V_P for a lateral FF-beam with composite support beams 8µm (4+4) longer than the needed 2nd mode lengths.

plot of Q versus dc-bias V_P for the 10.47 MHz device of Fig. 3. As shown, the Q is a strong function of the V_P-dependent frequency of the FF-beam, dropping off rapidly as the frequency of the FF-beam moves away from the second-mode resonance frequency of the composite support beams. This drop in Q is consistent with a mechanism where frequency mismatch between the beams moves the nodal point of the composite support beam away from the attachment location, thereby allowing increased energy transfer between the beams, and eventual loss to the anchors. Note that the drop in Q cannot be explained by a mere electrical stiffness variation with dc-bias V_P, which imparts a much smaller change in Q versus V_P, on the order of the dependency of f_o on V_P.

By purposely designing the supporting beams to be longer than second-mode, a Q-optimizable device is possible, for which V_P can be adjusted to lower the f_o until it corresponds to the second-mode frequency of the supports, at which point energy losses are nulled, and a maximum Q value attained. Figure 8 demonstrates this concept with a plot of Q versus V_P for a 10 MHz lateral FF-beam with longer supporting beams, clearly showing a peak in Q when V_P reaches the optimum value.

To further investigate the degree of isolation given by the second-mode supports, a series of lateral FF-beams with support beam lengths that deviate from the desired second-mode length were tested. Figure 9 presents measured plots of frequency f_o and Q versus the supporting beam length L_s for a 40µm-long FF-beam. Here, the frequency of the FF-beam is seen to increase from 13 MHz to 25 MHz when the supporting beam length is decreased from 25.6 µm to 5.6 µm. This is reasonable, since as L_s is reduced, the stiffness of the supporting beams increases, and begins to contribute more to the overall frequency of the device. That the frequency of the resonator beam approaches that of a clamped-clamped beam (with a length equal to the distance between node points), as L_s approaches zero is also expected, since the support beam begins to approach a rigid anchor at small lengths.

As expected, the Q for the FF-beam takes on its maximum value of 9,997 when the composite support beam lengths correspond to those that realize a second-mode

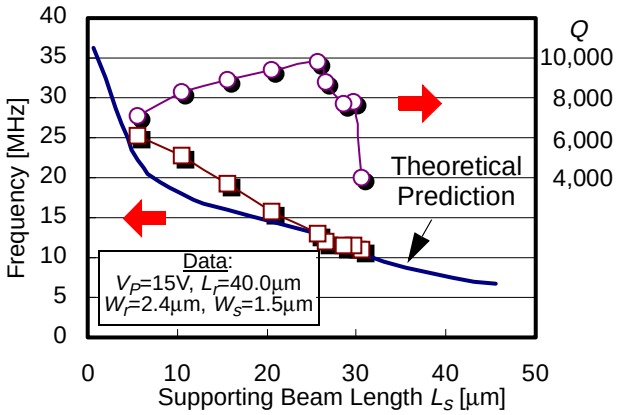

Fig. 9: Simulated and measured resonator Q and frequency versus supporting beam length for a 40µm long lateral FF-beam

resonance at the resonance frequency of the FF-beam. Interestingly, however, the plot of Q versus L_s is not symmetrical, having a much smaller slope for lengths deviating downwards from the optimum value than for upward deviations. The rather abrupt drop in Q for L_s>25.6 µm suggests that large amplitude off-resonance flexing of the support beam provides an efficient energy transfer path to the substrate.

V. CONCLUSIONS

Lateral free-free beam µmechanical resonators with second-mode isolating supports have been demonstrated with Q's ~10,000—very suitable for use in communications-grade oscillators and frequency filters. The utility of the isolating support design in maximizing Q was verified experimentally. However, the resonance frequency and Q of this resonator were found to be sensitive to errors in support beam length. In particular, overshoot errors (over the desired second-mode length) in support beam length were quite detrimental to the Q of the overall resonator. Finally, the use of metal electrodes in the capacitive transducers was found to be detrimental to the thermal stability of the resonance frequency due to thermal expansion of the electrodes, which made electrical stiffness a function of temperature. With adjustments to eliminate this electrode phenomenon, this resonator design should prove useful in improving the design flexibility of future µmechanical communications circuits, especially filters and oscillators.

Acknowledgment: This work was supported under DARPA Cooperative Agmt. No. F30602-97-2-0101.

References:

[1] K. Wang, *et al.*, *IEEE/ASME JMEMS*, vol. 9, no. 3, pp. 347-360, Sept. 2000.

[2] M. Roukes, *Hilton Head 2000*, pp. 367-376.

[3] C. T-C. Nguyen, *BCTM 2000*, pp. 142-149.

[4] F. D. Bannon III, *et al.*, *IEEE JSSC*, vol. 35, no. 4, pp. 512-526, April 2000.

[5] W.-T. Hsu, *et al.*, *MEMS'01*, pp 349-352.

[6] W.-T. Hsu, *et al.*, *Transducers'01*, this digest.